**Supplementary Materials**

## Strengthening high-stacking-fault-energy metals via parallelogram nanotwins

Yuefei Zhang[†,*], Jin Wang[†], Haiquan Shan[†], Kejie Zhao[‡,*]

[†]Institute of Microstructure and Property of Advanced Materials, Beijing University of Technology, Beijing 100124, P. R. China

[‡]School of Mechanical Engineering, Purdue University, West Lafayette, IN 47906, USA

*Correspondence should be addressed to Y. Z yfzhang@bjut.edu.cn and K. Z. kjzhao@purdue.edu

### Experimental methods

*Fabrication of nanotwinned Ni.* High-purity Ni foils samples with nanoscale twins were synthesized by means of electrodeposition on Cu substrate. The deposition was performed in a $NiSO_4$ and $H_3BO_3$ solution. The solution was maintained at a pH level of 1.0-3.5 and bath temperature of 30-80 °C. Electrodeposition was done with a two-electrode system with an electrolytic Ni sheet (99.8%) as anode and a Cu plate as cathode. During deposition, the electrolyte was mechanically stirred continuously. The optimized conditions on the twin density were obtained through a series of experiments in which various experimental parameters were tested (Tables S2-S6). The as-deposited Ni foils have in-plane dimensions of 30 mm by 30 mm and a thickness of 30 μm with a uniform microstructure.

*Microstructure and mechanical property characterization.* The as-deposited Ni foils were peeled off from Cu substrates. The microstructure of Ni foils was characterized by high-resolution transmission electron microscopy (JEOL 2010F) and conventional transmission electron microscopy (FEI G20). TEM specimens were double-jet electropolished in a solution of 25% nitric acid and 75% methanol at 15 V and -20 °C. Chemical composition analysis on both the as-deposited Ni foils and anode plate was made via X-Ray Fluorescence (Magix pw2403). XRD measurements were performed with a Bruker D8 X-ray detector. For the tensile test, the as-deposited Ni foils were cut into dog-bone-shaped specimens with a gauge length of 12 mm and width of 1 mm for tensile tests. The samples were tested on a CMT5000 testing system (MTS) with a specially designed clamping jig at a nominal strain rate $10^{-4}$ $s^{-1}$ at room temperature. The load cell capacity was 200 N. The surface and fracture morphology were imaged using a scanning electron microscopy (SEM, FEI Quanta 250, and JEOL 6500F).

*In-situ thermal stability characterization***.** *In-situ* thermal stability experiment was performed in a JEOL 2010 $LaB_6$ TEM operating at 200 kV. A Gatan double tilt-heating holder (Model 625) is used for heating. The maximum operating temperature for the holder is up to 1000 °C. A TEM sample was fabricated by electropolishing, and then was mounted on the TEM heating holder for observation up to 700 °C. The heating rate was 20 °C/min. There is no obvious change of morphology of NT Ni at temperatures below 400 °C.

**Table S1**. Electrodeposition conditions in the synthesis of Ni samples with parallel and parallelogram nanotwins. Each processing parameter is tested separately in the range listed in the table, and individual effect on the microstructure of as-deposited samples is shown in Tables S2-S5.

| Compounds | Parallel Nanotwin | Parallelogram Nanotwin |
|---|---|---|
| $NiSO_4 \cdot 6H_2O$(g/L) | 250-400 | 250-400 |
| $H_3BO_3$(g/L) | 20-35 | 20-35 |
| Temperature(℃) | 30-80 | 30-80 |
| pH Value | 1.0-3.5 | 1.0-3.5 |
| Current density (A/dm$^2$) | 7-20 | 7-20 |
| Pulse ($T_{on}$/$T_{off}$) (ms) | 20/20-1000 | On time $T_{on}$ |

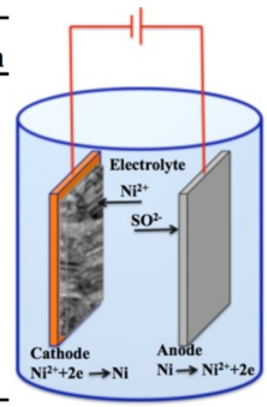

**Table S2.** Effect of the bath temperature on the average grain size, twin thickness, and twin length in the as-deposited samples.

| **Bath composition and conditions used for deposition** | |
|---|---|
| $NiSO_4 \cdot 6H_2O$ | 300(g/L) |
| $H_3BO_3$ | 30(g/L) |
| pH Value | 1.5 |
| Current Density | 15A/dm$^2$ |
| Pulse $T_{on}/T_{off}$ | 20ms/20ms |

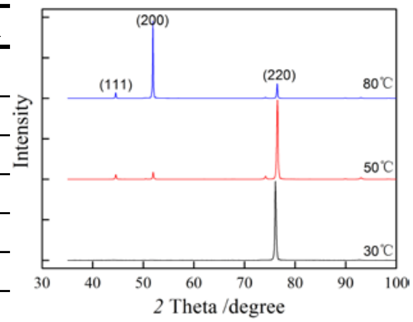


| Variable property settings | A | B | C |
|---|---|---|---|
| Temperature /℃ | 30 | 50 | 80 |
| Microstructure Feature | 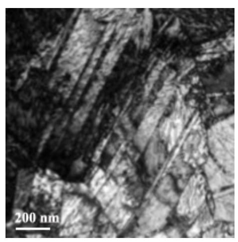  | 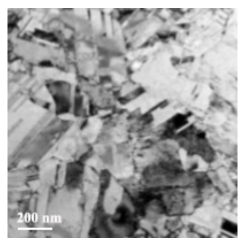  | 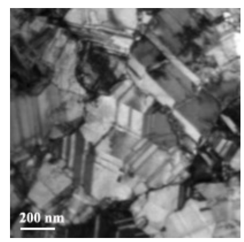  |
| Materials Properties | (nm) | (nm) | (nm) |
| Average Grain Size | 850 | 600 | 350 |
| Twin thickness | 55 | 35 | 30 |
| Twin length | 650 | 350 | 200 |

**Table S3.** Effect of the current density on the average grain size, twin thickness, and twin length in the as-deposited samples.

| **Bath composition and conditions used for deposition** | |
|---|---|
| $NiSO_4 \cdot 6H_2O$ | 350(g/L) |
| $H_3BO_3$ | 35(g/L) |
| pH Value | 1.5 |
| Temperature | 30℃ |
| Pulse$T_{on}$/$T_{off}$ | 20ms/1000ms |

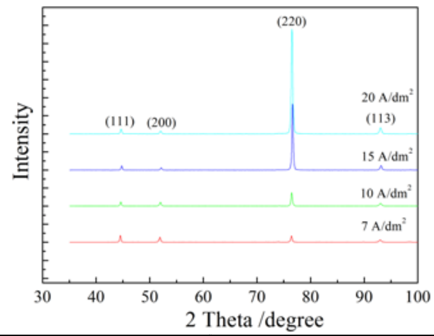


| Variable property settings | A | B | C | D |
|---|---|---|---|---|
| Current density （$A/dm^2$） | 7 | 10 | 15 | 20 |
| Typical Microstructure Feature | 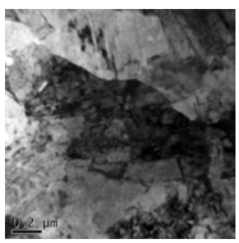 | 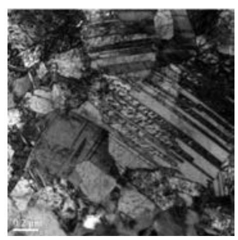 | 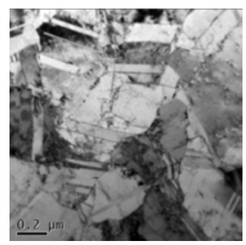 | 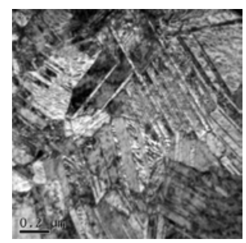 |
| Materials Properties | (nm) | (nm) | (nm) | (nm) |
| Average Grain Size | 600 | 600 | 450 | 300 |
| Twin thickness | 110 | 80 | 50 | 30 |
| Twin length | 550 | 500 | 400 | 300 |

**Table S4.** 1 Effect of the $Ni^{2+}$ concentration on the average grain size, twin thickness, and twin length in the as-deposited samples.

| **Bath composition and conditions used for deposition** | |
|---|---|
| $H_3BO_3$ | 35(g/L) |
| pH Value | 2.0 |
| Temperature | 30℃ |
| Pulse$T_{on}/T_{off}$ | 20ms/0 |
| Current density | $15A/dm^2$ |

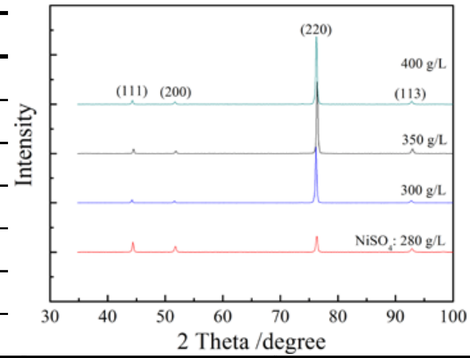


| Variable property settings | A | B | C | D |
|---|---|---|---|---|
| $NiSO_4 \cdot 6H_2O$(g/L) | 280 | 300 | 350 | 400 |
| Typical Microstructure Feature | 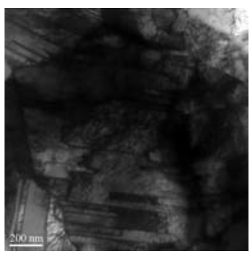 | 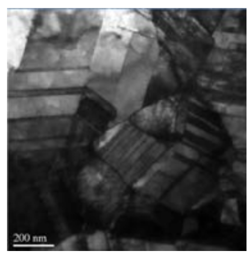 | 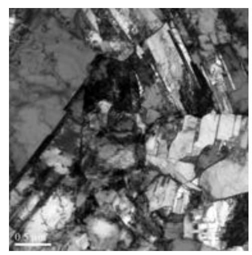 | 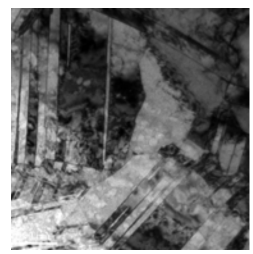 |
| Materials Properties | (nm) | (nm) | (nm) | (nm) |
| Average Grain Size | 550 | 400 | 500 | 450 |
| Twin thickness | 85 | 50 | 40 | 35 |
| Twin length | 500 | 400 | 450 | 450 |

**Table S5.** Effect of the $T_{on}/T_{off}$ on the average grain size, twin thickness, and twin length in the as-deposited samples.

| **Bath composition and conditions used for deposition** | |
|---|---|
| $NiSO_4 \cdot 6H_2O$ | 300(g/L) |
| $H_3BO_3$ | 35(g/L) |
| pH Value | 2.0 |
| Temperature | 30℃ |
| Current density | 15A/$dm^2$ |

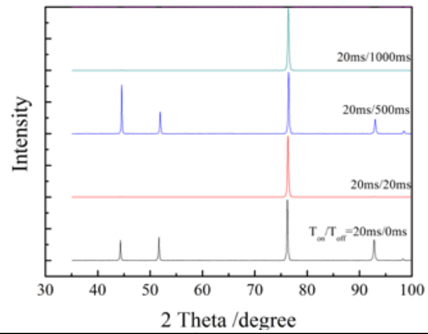


| Variable property settings | A | B | C | D |
|---|---|---|---|---|
| Pulse $T_{on}/T_{off}$ | 20ms/0 | 20ms/20ms | 20ms/500ms | 20ms/1000ms |
| Typical Microstructure Feature | 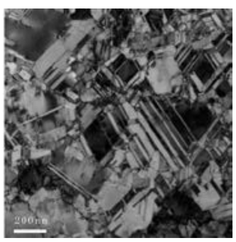 | 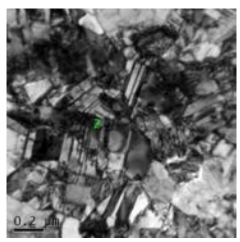 | 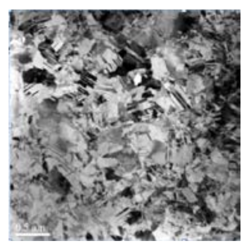 | 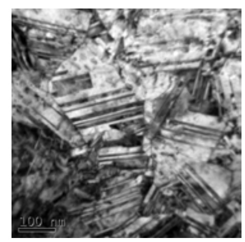 |
| Materials Properties | (nm) | (nm) | (nm) | (nm) |
| Average Grain Size | 600 | 500 | 400 | 350 |
| Twin thickness | 50 | 60 | 50 | 30 |
| Twin length | 300 | 400 | 200 | 300 |

**Table S6**. Qualitative effects of the variation of experimental parameters on the twin density and average grain size in the as-deposited samples. The up-arrow represents the increase of the quantity, down-arrow the decrease, and left-right arrow no obvious change. Quantification of each individual effect is shown in Tables S2-S5.

| **Electrolyte:** | **Temperature** | **pH Value** | **Current density** | **$T_{off}$ time** | **$Ni^{2+}$ concentration** |
|---|---|---|---|---|---|
| **$NiSO_4+H_3BO_3$** | ↑ | ↑ | ↑ | ↑ | ↑ |
| **Twin density** | ↑ | ↔ | ↑ | ↑ | ↑ |
| **Grain Size** | ↓ | ↔ | ↓ | ↓ | ↓ |

a b

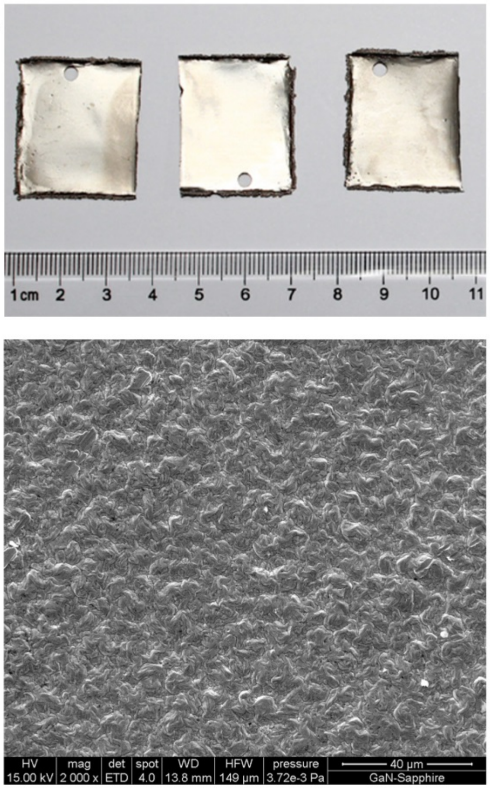


c

| Samples | Compound Name | Conc. (%) |
|---|---|---|
| 1 | Ni | 99.9 |
| | Si | 0.0788 |
| | S | 0.0191 |
| 2 | Ni | 99.9 |
| | Co | 0.124 |
| | S | 0.00213 |
| 3 | Ni | 99.9 |
| | Co | 0.106 |
| Anode Ni | Ni | 99.8 |
| | Fe | 0.0768 |
| | S | 0.0689 |
| | Si | 0.0601 |
| | P | 0.0346 |

**Figure S1.** Morphology and composition of as-deposited Ni foils. (a) Ni foils synthesized by electrodeposition**.** The peeled-off samples have in-plane dimensions of 30 mm × 30 mm and thickness of 30 μm. (b) A SEM image shows the surface morphology. (c) Composition analysis indicates the high purity of as-deposited samples.

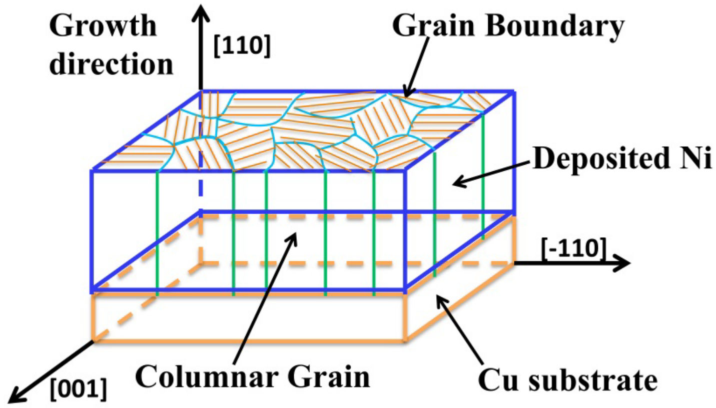


**Figure S2.** Schematics of the columnar grain structure and the growth direction of Ni samples.

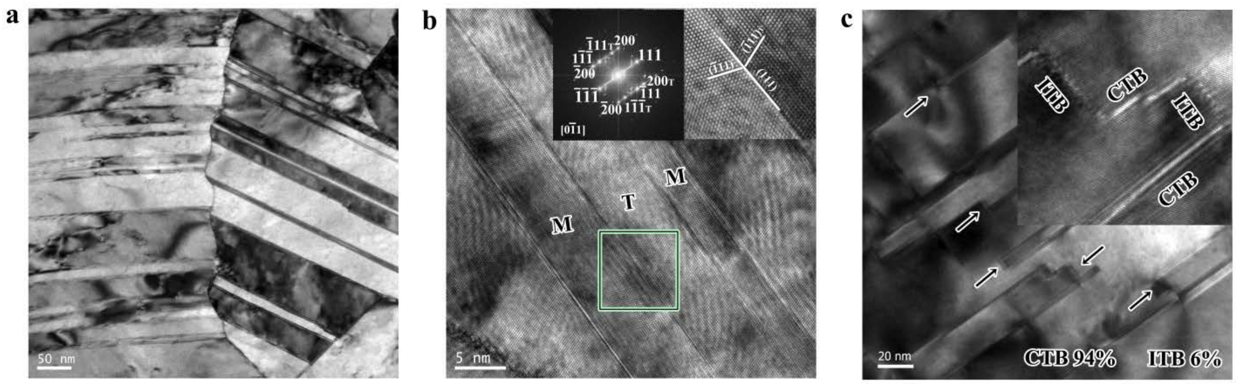


**Figure S3.** High-resolution TEM images show the microstructure of parallel nanotwins. (a) Nanotwins in {111} planes are parallel to each other in Ni foils synthesized by pulsed electrodeposition. (b) HRTEM image and the electron diffraction pattern (inset) show the twinning sequence of matrix-twin-matrix. (c) Coexistence of Σ3{111} CTBs and Σ3{112} ITBs. The arrows indicate the ITBs.

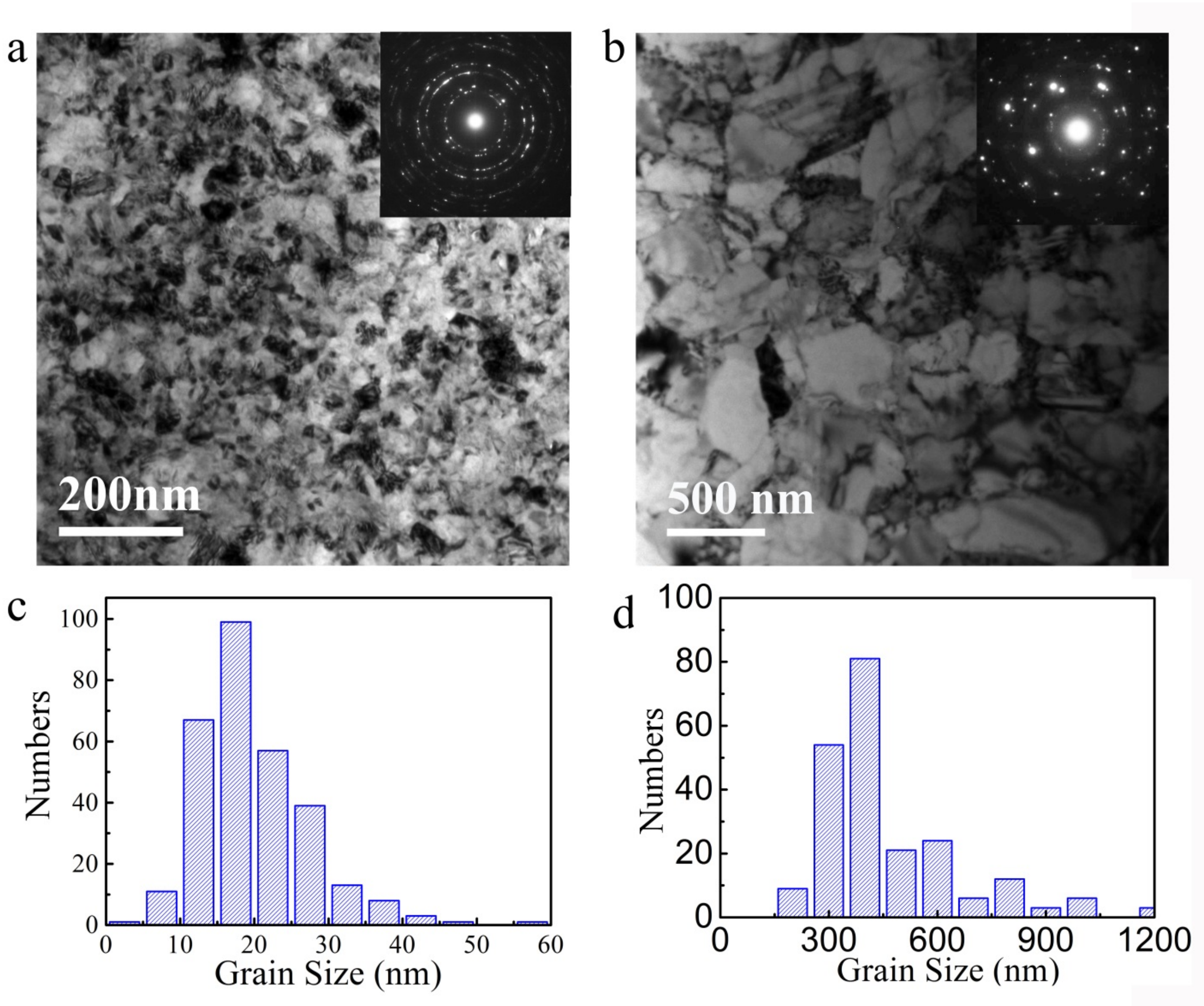


**Figure S4.** Microstructure and statistics of grain size. (a) and (c) nanocrystalline Ni. (b) and (d) coarse-grained polycrystalline Ni.

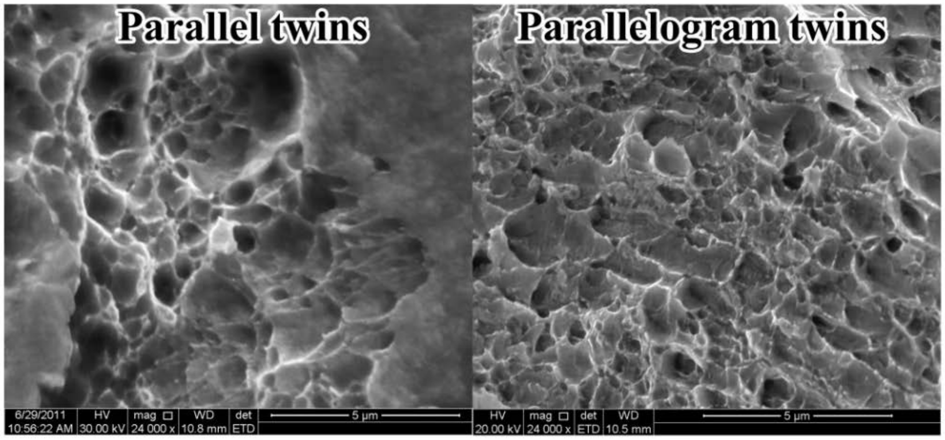


**Figure S5.** SEM images show the ductile dimpled surface and microvoid coalescence upon fracture of nanotwinned Ni.

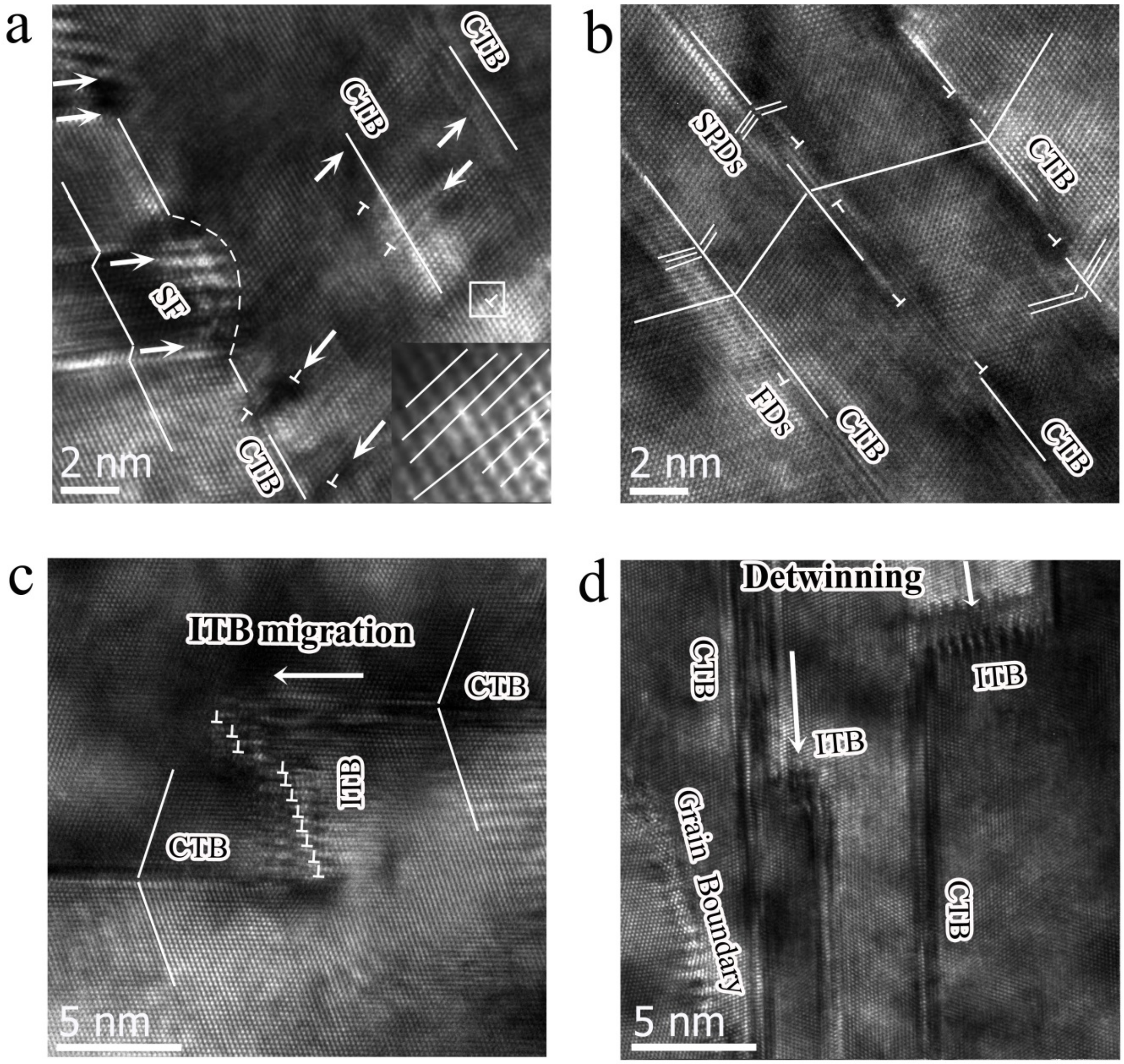


**Figure S6**. Deformation mechanisms of nanotwinned Ni examined by post-mortem HRTEM. (a) Dislocations pile-up at CTBs and transmit across the twin boundaries. The interactions between dislocations with CTBs generate well populations of stacking faults and distort the twin boundaries. The arrows indicate stacking faults. (b) Glissile Shockley partial dislocations slip along twin planes and mediate the migration of CTBs. Sessile Frank dislocations are left at CTBs. (c) Migration of ITB through collective motions of dislocations within the grain. (d) Detwinning accompanied with the migration of Σ3{112} ITBs.